

Analysis of Coupled Dynamics of Molten Salt Reactors



Valentino Di Marcello*, Antonio Cammi, Lelio Luzzi
 Department of Energy – Enrico Fermi Center for Nuclear Studies (CeSNEF), Politecnico di Milano
 Address: via Ponzio 34/3 – 20133 Milano (Italy)
 * Corresponding author. E-mail address: valentino.dimarcello@mail.polimi.it; tel.: +39 02 2399 6326

SUMMARY

This work presents a preliminary analysis of the coupled thermo-hydrodynamics and neutronics of circulating nuclear fuel systems like the thermal Molten Salt Reactor (MSR), one of the "Generation IV International Forum" concepts [1]. This kind of nuclear reactor adopts a molten salt mixture, which flows up through channels in a graphite moderated core and plays the role of both heat generator and coolant [2]. In the core fission occurs within the flowing fuel salt, which then circulates in a primary heat exchanger, where the heat is transferred to a secondary liquid salt coolant; the fuel salt then flows back to the reactor core (see Figure 1).

MSRs are featured by a strong coupling between neutronics and thermo-hydrodynamics, which can be properly treated by means of a multi-physics approach. In this paper a simple 2-D geometry, representing a typical channel of a sub-critical MSR that comprises both the flowing molten salt fuel and the graphite matrix, has been considered. Physics of such system can be modelled by means of eight coupled partial differential equations, describing the fluid motion and the balances of energy, neutrons and precursors (see Table 1). With reference to this complex and highly non linear environment, COMSOL® confirmed as an adequate tool to catch some relevant features of both the steady state and the dynamic behaviour of the considered MSR channel. Analyses have been carried out for both laminar and turbulent flow regimes, focusing on the influence that graphite has on such system, in the light of a thermo-hydrodynamic validation discussed in a parallel work on the basis of both an analytical framework and a code-to-code (COMSOL® vs. FLUENT®) comparison [3]. In particular, the time constants of some physical quantities have been discussed: namely, the neutron flux, the precursors concentration, the fluid temperature and the graphite temperature, whose time evolution is of extreme interest for the investigation of the dynamic behaviour as well as of the most appropriate control strategy to be adopted in the current development of Molten Salt Reactors for Generation IV.

In short, this study has provided important information about the channel behaviour of a sub-critical MSR and paves the way for further progress concerning more complex and design-oriented simulations, which should consider more representative geometries of the power channels (if not of the whole reactor core) and more details in the neutronic modelling of both the molten salt and the graphite, as well as of their "nuclear" interaction.

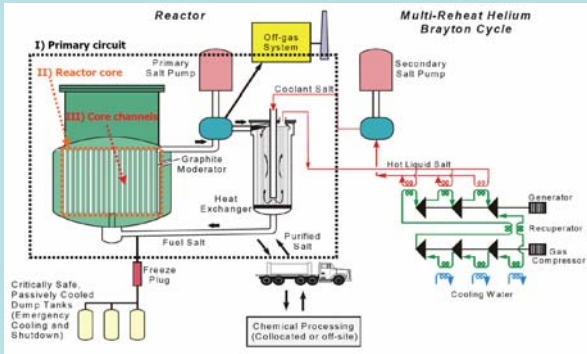


Figure 1. Typical layout of a nuclear power plant based on thermal (graphite moderated) MSR technology (from Ref. [2]): I) primary circuit; II) reactor core; III) core channels.

MULTI-PHYSICS MODEL

The multi-physics modelling adopted in this work consists of eight coupled partial differential equations describing the fluid motion (RANS – Reynolds Averaged Navier-Stokes equations with the standard k-ε turbulence model), the energy balance, the neutron and the precursors balances (see Table 1).

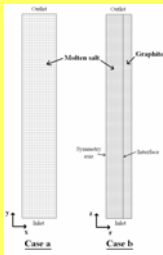


Figure 2. Geometry and mesh structure of the analyzed systems.

Geometry

Two different 2-D geometries have been considered for the analyses, i.e.: a Cartesian (x,y) geometry (0.58 m x 3.46 m rectangular box) representing a finite region of a sub-critical reactor (case a, as in Ref. [4]); an axial symmetric cylindrical geometry (r,z) representing a MSR (sub-critical) core channel (case b, shown in Figure 2). The channel considered in the present work is featured by an inner and outer graphite radius of 0.29 m and 0.43 m, respectively, and a height of 3.46 m.

It is worth noting that the size of the channel, in which the molten salt circulates, is a key design issue for MSRs, influencing relevant parameters like the moderation ratio, the total reactivity feedback coefficient, the breeding ratio, the graphite lifetime and the initial fissile inventory; a critical discussion of such effects, which are out of the scope of this work, can be found in [2].

Fluid motion:	Neutronics:
$\rho \frac{\partial u}{\partial t} + \rho u \frac{\partial u}{\partial x} + \rho v \frac{\partial u}{\partial y} = -\frac{\partial p}{\partial x} + \mu \nabla^2 u + \rho \left(\eta_1 \frac{\partial u}{\partial x} + \eta_2 \frac{\partial v}{\partial y} \right) - \frac{\partial}{\partial x} (v u)$	A interface heat transfer surface
$\rho \frac{\partial v}{\partial t} + \rho u \frac{\partial v}{\partial x} + \rho v \frac{\partial v}{\partial y} = -\frac{\partial p}{\partial y} + \mu \nabla^2 v + \rho \left(\eta_1 \frac{\partial v}{\partial x} + \eta_2 \frac{\partial v}{\partial y} \right) - \frac{\partial}{\partial y} (v u)$	c precursors concentration
$\rho \frac{\partial T}{\partial t} + \rho u \frac{\partial T}{\partial x} + \rho v \frac{\partial T}{\partial y} = \nabla \cdot (k \nabla T) + \rho c_p \left(\eta_1 \frac{\partial T}{\partial x} + \eta_2 \frac{\partial T}{\partial y} \right) - \frac{\partial}{\partial x} (v T) - \frac{\partial}{\partial y} (v T)$	$C_{p,f}$ specific heat capacity of fluid
$\rho \frac{\partial T_g}{\partial t} + \rho u \frac{\partial T_g}{\partial x} + \rho v \frac{\partial T_g}{\partial y} = \nabla \cdot (k_g \nabla T_g) + \rho c_{p,g} \left(\eta_1 \frac{\partial T_g}{\partial x} + \eta_2 \frac{\partial T_g}{\partial y} \right) - \frac{\partial}{\partial x} (v T_g) - \frac{\partial}{\partial y} (v T_g)$	$C_{p,g}$ specific heat capacity of graphite
$\rho \frac{\partial \phi}{\partial t} + \rho u \frac{\partial \phi}{\partial x} + \rho v \frac{\partial \phi}{\partial y} = \nabla \cdot (D \nabla \phi) + \rho \Sigma_f \phi - \rho \Sigma_a \phi + \rho \lambda c$	C_{μ} k-ε model constant
$\rho \frac{\partial c}{\partial t} + \rho u \frac{\partial c}{\partial x} + \rho v \frac{\partial c}{\partial y} = \nabla \cdot (D_c \nabla c) + \rho \lambda c - \rho \Sigma_a c$	$C_{\mu,2}$ k-ε model constant
$\rho \frac{\partial k}{\partial t} + \rho u \frac{\partial k}{\partial x} + \rho v \frac{\partial k}{\partial y} = \nabla \cdot (D_k \nabla k) + \rho P_k - \rho \epsilon$	$C_{\mu,3}$ precursors diffusion coefficient
$\rho \frac{\partial \epsilon}{\partial t} + \rho u \frac{\partial \epsilon}{\partial x} + \rho v \frac{\partial \epsilon}{\partial y} = \nabla \cdot (D_\epsilon \nabla \epsilon) + \rho P_\epsilon - \rho \epsilon$	D_c neutron diffusion coefficient
$\rho \frac{\partial \eta_1}{\partial t} + \rho u \frac{\partial \eta_1}{\partial x} + \rho v \frac{\partial \eta_1}{\partial y} = \nabla \cdot (D_{\eta_1} \nabla \eta_1) + \rho P_{\eta_1} - \rho \eta_1$	F_x horizontal component of volume force
$\rho \frac{\partial \eta_2}{\partial t} + \rho u \frac{\partial \eta_2}{\partial x} + \rho v \frac{\partial \eta_2}{\partial y} = \nabla \cdot (D_{\eta_2} \nabla \eta_2) + \rho P_{\eta_2} - \rho \eta_2$	F_y vertical component of volume force
$\rho \frac{\partial \eta_3}{\partial t} + \rho u \frac{\partial \eta_3}{\partial x} + \rho v \frac{\partial \eta_3}{\partial y} = \nabla \cdot (D_{\eta_3} \nabla \eta_3) + \rho P_{\eta_3} - \rho \eta_3$	g gravity acceleration
$\rho \frac{\partial \eta_4}{\partial t} + \rho u \frac{\partial \eta_4}{\partial x} + \rho v \frac{\partial \eta_4}{\partial y} = \nabla \cdot (D_{\eta_4} \nabla \eta_4) + \rho P_{\eta_4} - \rho \eta_4$	h heat transfer coefficient
$\rho \frac{\partial \eta_5}{\partial t} + \rho u \frac{\partial \eta_5}{\partial x} + \rho v \frac{\partial \eta_5}{\partial y} = \nabla \cdot (D_{\eta_5} \nabla \eta_5) + \rho P_{\eta_5} - \rho \eta_5$	I identity matrix (2x2)
$\rho \frac{\partial \eta_6}{\partial t} + \rho u \frac{\partial \eta_6}{\partial x} + \rho v \frac{\partial \eta_6}{\partial y} = \nabla \cdot (D_{\eta_6} \nabla \eta_6) + \rho P_{\eta_6} - \rho \eta_6$	k turbulent kinetic energy
$\rho \frac{\partial \eta_7}{\partial t} + \rho u \frac{\partial \eta_7}{\partial x} + \rho v \frac{\partial \eta_7}{\partial y} = \nabla \cdot (D_{\eta_7} \nabla \eta_7) + \rho P_{\eta_7} - \rho \eta_7$	k_f thermal conductivity of fluid
$\rho \frac{\partial \eta_8}{\partial t} + \rho u \frac{\partial \eta_8}{\partial x} + \rho v \frac{\partial \eta_8}{\partial y} = \nabla \cdot (D_{\eta_8} \nabla \eta_8) + \rho P_{\eta_8} - \rho \eta_8$	k_g thermal conductivity of graphite
$\rho \frac{\partial \eta_9}{\partial t} + \rho u \frac{\partial \eta_9}{\partial x} + \rho v \frac{\partial \eta_9}{\partial y} = \nabla \cdot (D_{\eta_9} \nabla \eta_9) + \rho P_{\eta_9} - \rho \eta_9$	$k_{g,eff}$ turbulent thermal conductivity
$\rho \frac{\partial \eta_{10}}{\partial t} + \rho u \frac{\partial \eta_{10}}{\partial x} + \rho v \frac{\partial \eta_{10}}{\partial y} = \nabla \cdot (D_{\eta_{10}} \nabla \eta_{10}) + \rho P_{\eta_{10}} - \rho \eta_{10}$	m_g mass of graphite
$\rho \frac{\partial \eta_{11}}{\partial t} + \rho u \frac{\partial \eta_{11}}{\partial x} + \rho v \frac{\partial \eta_{11}}{\partial y} = \nabla \cdot (D_{\eta_{11}} \nabla \eta_{11}) + \rho P_{\eta_{11}} - \rho \eta_{11}$	n neutrons
$\rho \frac{\partial \eta_{12}}{\partial t} + \rho u \frac{\partial \eta_{12}}{\partial x} + \rho v \frac{\partial \eta_{12}}{\partial y} = \nabla \cdot (D_{\eta_{12}} \nabla \eta_{12}) + \rho P_{\eta_{12}} - \rho \eta_{12}$	n_0 precursor of fluid
$\rho \frac{\partial \eta_{13}}{\partial t} + \rho u \frac{\partial \eta_{13}}{\partial x} + \rho v \frac{\partial \eta_{13}}{\partial y} = \nabla \cdot (D_{\eta_{13}} \nabla \eta_{13}) + \rho P_{\eta_{13}} - \rho \eta_{13}$	Pr_t turbulent Prandtl number
$\rho \frac{\partial \eta_{14}}{\partial t} + \rho u \frac{\partial \eta_{14}}{\partial x} + \rho v \frac{\partial \eta_{14}}{\partial y} = \nabla \cdot (D_{\eta_{14}} \nabla \eta_{14}) + \rho P_{\eta_{14}} - \rho \eta_{14}$	Q_{ext} amplitude of external neutron source
$\rho \frac{\partial \eta_{15}}{\partial t} + \rho u \frac{\partial \eta_{15}}{\partial x} + \rho v \frac{\partial \eta_{15}}{\partial y} = \nabla \cdot (D_{\eta_{15}} \nabla \eta_{15}) + \rho P_{\eta_{15}} - \rho \eta_{15}$	$Q_{ext,g}$ energy source term within graphite
$\rho \frac{\partial \eta_{16}}{\partial t} + \rho u \frac{\partial \eta_{16}}{\partial x} + \rho v \frac{\partial \eta_{16}}{\partial y} = \nabla \cdot (D_{\eta_{16}} \nabla \eta_{16}) + \rho P_{\eta_{16}} - \rho \eta_{16}$	$Q_{ext,s}$ external neutron source
$\rho \frac{\partial \eta_{17}}{\partial t} + \rho u \frac{\partial \eta_{17}}{\partial x} + \rho v \frac{\partial \eta_{17}}{\partial y} = \nabla \cdot (D_{\eta_{17}} \nabla \eta_{17}) + \rho P_{\eta_{17}} - \rho \eta_{17}$	$Q_{ext,t}$ time
$\rho \frac{\partial \eta_{18}}{\partial t} + \rho u \frac{\partial \eta_{18}}{\partial x} + \rho v \frac{\partial \eta_{18}}{\partial y} = \nabla \cdot (D_{\eta_{18}} \nabla \eta_{18}) + \rho P_{\eta_{18}} - \rho \eta_{18}$	T_0 reference temperature
$\rho \frac{\partial \eta_{19}}{\partial t} + \rho u \frac{\partial \eta_{19}}{\partial x} + \rho v \frac{\partial \eta_{19}}{\partial y} = \nabla \cdot (D_{\eta_{19}} \nabla \eta_{19}) + \rho P_{\eta_{19}} - \rho \eta_{19}$	T_g temperature of graphite
$\rho \frac{\partial \eta_{20}}{\partial t} + \rho u \frac{\partial \eta_{20}}{\partial x} + \rho v \frac{\partial \eta_{20}}{\partial y} = \nabla \cdot (D_{\eta_{20}} \nabla \eta_{20}) + \rho P_{\eta_{20}} - \rho \eta_{20}$	T_s temperature of salt
$\rho \frac{\partial \eta_{21}}{\partial t} + \rho u \frac{\partial \eta_{21}}{\partial x} + \rho v \frac{\partial \eta_{21}}{\partial y} = \nabla \cdot (D_{\eta_{21}} \nabla \eta_{21}) + \rho P_{\eta_{21}} - \rho \eta_{21}$	u_0 average velocity of neutrons
$\rho \frac{\partial \eta_{22}}{\partial t} + \rho u \frac{\partial \eta_{22}}{\partial x} + \rho v \frac{\partial \eta_{22}}{\partial y} = \nabla \cdot (D_{\eta_{22}} \nabla \eta_{22}) + \rho P_{\eta_{22}} - \rho \eta_{22}$	α coefficient of thermal expansion
$\rho \frac{\partial \eta_{23}}{\partial t} + \rho u \frac{\partial \eta_{23}}{\partial x} + \rho v \frac{\partial \eta_{23}}{\partial y} = \nabla \cdot (D_{\eta_{23}} \nabla \eta_{23}) + \rho P_{\eta_{23}} - \rho \eta_{23}$	β fraction of neutrons emitted by precursors
$\rho \frac{\partial \eta_{24}}{\partial t} + \rho u \frac{\partial \eta_{24}}{\partial x} + \rho v \frac{\partial \eta_{24}}{\partial y} = \nabla \cdot (D_{\eta_{24}} \nabla \eta_{24}) + \rho P_{\eta_{24}} - \rho \eta_{24}$	γ turbulent dissipation rate
$\rho \frac{\partial \eta_{25}}{\partial t} + \rho u \frac{\partial \eta_{25}}{\partial x} + \rho v \frac{\partial \eta_{25}}{\partial y} = \nabla \cdot (D_{\eta_{25}} \nabla \eta_{25}) + \rho P_{\eta_{25}} - \rho \eta_{25}$	λ heat produced per fission reaction
$\rho \frac{\partial \eta_{26}}{\partial t} + \rho u \frac{\partial \eta_{26}}{\partial x} + \rho v \frac{\partial \eta_{26}}{\partial y} = \nabla \cdot (D_{\eta_{26}} \nabla \eta_{26}) + \rho P_{\eta_{26}} - \rho \eta_{26}$	μ dynamic viscosity of fluid
$\rho \frac{\partial \eta_{27}}{\partial t} + \rho u \frac{\partial \eta_{27}}{\partial x} + \rho v \frac{\partial \eta_{27}}{\partial y} = \nabla \cdot (D_{\eta_{27}} \nabla \eta_{27}) + \rho P_{\eta_{27}} - \rho \eta_{27}$	ν eddy viscosity
$\rho \frac{\partial \eta_{28}}{\partial t} + \rho u \frac{\partial \eta_{28}}{\partial x} + \rho v \frac{\partial \eta_{28}}{\partial y} = \nabla \cdot (D_{\eta_{28}} \nabla \eta_{28}) + \rho P_{\eta_{28}} - \rho \eta_{28}$	ω decay constant of precursors
$\rho \frac{\partial \eta_{29}}{\partial t} + \rho u \frac{\partial \eta_{29}}{\partial x} + \rho v \frac{\partial \eta_{29}}{\partial y} = \nabla \cdot (D_{\eta_{29}} \nabla \eta_{29}) + \rho P_{\eta_{29}} - \rho \eta_{29}$	ω_0 average number of neutrons per fission
$\rho \frac{\partial \eta_{30}}{\partial t} + \rho u \frac{\partial \eta_{30}}{\partial x} + \rho v \frac{\partial \eta_{30}}{\partial y} = \nabla \cdot (D_{\eta_{30}} \nabla \eta_{30}) + \rho P_{\eta_{30}} - \rho \eta_{30}$	ω_f fission macroscopic cross section
$\rho \frac{\partial \eta_{31}}{\partial t} + \rho u \frac{\partial \eta_{31}}{\partial x} + \rho v \frac{\partial \eta_{31}}{\partial y} = \nabla \cdot (D_{\eta_{31}} \nabla \eta_{31}) + \rho P_{\eta_{31}} - \rho \eta_{31}$	ρ density of fluid
$\rho \frac{\partial \eta_{32}}{\partial t} + \rho u \frac{\partial \eta_{32}}{\partial x} + \rho v \frac{\partial \eta_{32}}{\partial y} = \nabla \cdot (D_{\eta_{32}} \nabla \eta_{32}) + \rho P_{\eta_{32}} - \rho \eta_{32}$	ρ_g reference density of fluid
$\rho \frac{\partial \eta_{33}}{\partial t} + \rho u \frac{\partial \eta_{33}}{\partial x} + \rho v \frac{\partial \eta_{33}}{\partial y} = \nabla \cdot (D_{\eta_{33}} \nabla \eta_{33}) + \rho P_{\eta_{33}} - \rho \eta_{33}$	ρ_s density of graphite
$\rho \frac{\partial \eta_{34}}{\partial t} + \rho u \frac{\partial \eta_{34}}{\partial x} + \rho v \frac{\partial \eta_{34}}{\partial y} = \nabla \cdot (D_{\eta_{34}} \nabla \eta_{34}) + \rho P_{\eta_{34}} - \rho \eta_{34}$	ρ_t density of graphite
$\rho \frac{\partial \eta_{35}}{\partial t} + \rho u \frac{\partial \eta_{35}}{\partial x} + \rho v \frac{\partial \eta_{35}}{\partial y} = \nabla \cdot (D_{\eta_{35}} \nabla \eta_{35}) + \rho P_{\eta_{35}} - \rho \eta_{35}$	$\rho_{t,eff}$ k-ε model constant
$\rho \frac{\partial \eta_{36}}{\partial t} + \rho u \frac{\partial \eta_{36}}{\partial x} + \rho v \frac{\partial \eta_{36}}{\partial y} = \nabla \cdot (D_{\eta_{36}} \nabla \eta_{36}) + \rho P_{\eta_{36}} - \rho \eta_{36}$	$\rho_{t,2}$ k-ε model constant
$\rho \frac{\partial \eta_{37}}{\partial t} + \rho u \frac{\partial \eta_{37}}{\partial x} + \rho v \frac{\partial \eta_{37}}{\partial y} = \nabla \cdot (D_{\eta_{37}} \nabla \eta_{37}) + \rho P_{\eta_{37}} - \rho \eta_{37}$	$\rho_{t,3}$ k-ε model constant
$\rho \frac{\partial \eta_{38}}{\partial t} + \rho u \frac{\partial \eta_{38}}{\partial x} + \rho v \frac{\partial \eta_{38}}{\partial y} = \nabla \cdot (D_{\eta_{38}} \nabla \eta_{38}) + \rho P_{\eta_{38}} - \rho \eta_{38}$	$\rho_{t,4}$ absorption macroscopic cross section
$\rho \frac{\partial \eta_{39}}{\partial t} + \rho u \frac{\partial \eta_{39}}{\partial x} + \rho v \frac{\partial \eta_{39}}{\partial y} = \nabla \cdot (D_{\eta_{39}} \nabla \eta_{39}) + \rho P_{\eta_{39}} - \rho \eta_{39}$	τ_g time constant of graphite
$\rho \frac{\partial \eta_{40}}{\partial t} + \rho u \frac{\partial \eta_{40}}{\partial x} + \rho v \frac{\partial \eta_{40}}{\partial y} = \nabla \cdot (D_{\eta_{40}} \nabla \eta_{40}) + \rho P_{\eta_{40}} - \rho \eta_{40}$	τ_s neutron flux

Table 1. System of equations and material properties (for the molten salt from Ref. [5], for the graphite from Ref. [6]).

Main References

- [1] A Technology Roadmap for Generation IV Nuclear Energy Systems, issued by the U.S. DOE Nuclear Energy Research Advisory Committee and the Generation IV International Forum, GIF-002-00 (2002).
- [2] C.W. Forsberg et al., Liquid Salt Applications and Molten Salt Reactors, Proceedings of ICAPP '07, Nice, France, May 13-18 (2007).
- [3] V. Di Marcello, A. Cammi, L. Luzzi, Analysis of Thermal-Hydraulic Behaviour of the Molten Salt Nuclear Fuel, Proceedings of the International Conference Nuclear Energy for New Europe 2008, Portoroz, Slovenia, September 8-11 (2008).
- [4] A. Cammi, V. Di Marcello, L. Luzzi, Modelling of Circulating Nuclear Fuels with COMSOL Multiphysics, Proceedings of the European COMSOL Conference 2007, Grenoble, France, October 23-24, 2007, vol. 1, pp. 380-386 (2007).
- [5] G. Lapenta, Mathematical and Numerical Models for the Coupling of Neutronics and Thermo-Hydrodynamics in Circulating Fuel Nuclear Reactors, in Nuclear Reactor Physics, pp. 195-210. CLUT, Turin (2005).
- [6] P. Mandin, H. Belachgar, A. Nuttin, G. Picard, Hydrothermal Modelling for the Molten Salt Reactor Design Optimisation, Proceedings of NURETH-11, Paper 227, Avignon, France, October 2-6 (2005).

RESULTS

The initial state assumes the reactor to be at zero power, with an established hydrodynamic pattern. A start-up transient has been simulated, adopting for the external neutron source a cosine spatial shape [4]. The physics of the system brings to the attainment of a steady state by relaxing the initial conditions. Simulations have been carried out for both cases a and b in turbulent flow with a Reynolds number (Re) equal to $8 \cdot 10^4$. Moreover, for the case a, further analyses have been performed with $Re = 8 \cdot 10^5$ and compared to the simulations with laminar flow of Ref. [4].

Case a

In laminar flow the buoyancy effect (according to the Boussinesq approximation) is more important than in the turbulent one because the fluid temperature is higher, and the fluid recirculation is more evident; as a consequence, the precursors are more concentrated in the upper part of the domain for the turbulent case (see Figure 3). The different flow regimes significantly influence the dynamic behaviour of the system, as shown in Figure 4: the time constant of the fluid temperature in the two considered turbulent regimes is lower than in laminar flow, showing a relevant dependence on the imposed inlet velocity, which also affects the precursors time evolution.

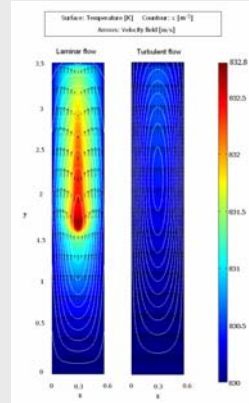


Figure 3. Case a: temperature (surface), precursors concentration (contour) and velocity field (arrows) for steady state conditions in both laminar (from Ref. [4]) and turbulent (present work, with $Re = 8 \cdot 10^4$) flows.

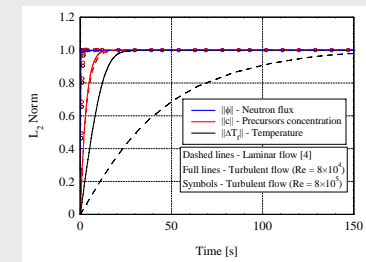


Figure 4. Case a: system time evolution.

Case b

A specific feature of the graphite + molten salt (fuel/coolant) system, unlike the externally cooled solid fuel rods adopted in the conventional nuclear reactors, is shown in Figure 5: initially, the heat is transferred from the fuel/coolant to the graphite matrix, but a situation is eventually reached where the radial heat flux is inverted between them. This behaviour is clear in Figure 6: in the simulated transient, and in any case in steady state operation, the graphite temperature results higher than the molten salt temperature, due to the assumed heat transfer boundary conditions. The radial temperature profile of the graphite is affected by the heat transfer coefficient (h) with the molten salt: the value of the Nusselt number ($Nu = 461$) obtained in this case results in a very good agreement with that achievable by means of the well-known Dittus-Boelter correlation, as thoroughly discussed in [3]. As shown in Figure 7, the neutron flux, the precursors concentration, the fluid and graphite temperatures exhibit very different time scales, which are relevant for the operation and the control of the reactor and, more in general, of the overall nuclear power conversion system, as discussed in [4]. It must be noticed that the time constant of graphite is much greater than the other ones; moreover, its order of magnitude can be caught by using the simple formula for τ_g given in Table 1.

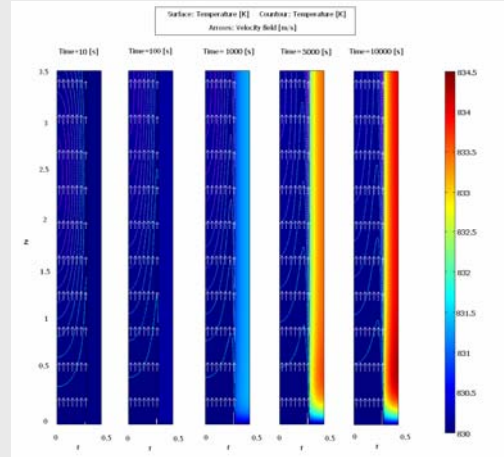


Figure 5. Temperature (surface and contour) and velocity field (arrows) at different times.

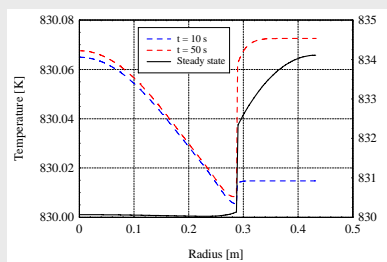


Figure 6. Case b: temperature radial profiles on the channel mid-plane at different times (dashed lines – left axis) compared to the steady state solution (full line – right axis).

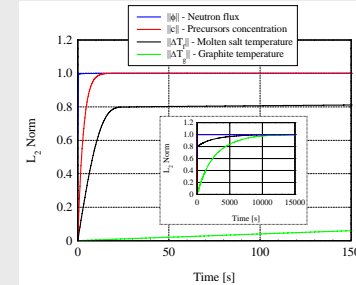


Figure 7. Case b: system time evolution.